



Physical Properties and Electrochemical Features of Lithium Nickel-Cobalt Oxide Cathode Materials Prepared at Moderate Temperature

L. EL-FARH, M. MASSOT, M. LEMAL & C. JULIEN

Laboratoire des Milieux Désordonnés et Hétérogènes, UMR-CNRS 7603, Université Pierre et Marie Curie, 4 place Jussieu, 75252 Paris cedex 05, France

S. CHITRA, P. KALYANI, T. MOHAN & R. GANGADHARAN

Lithium Batteries Division, Central Electrochemical Research Institute, Karaikudi, 630006 India

Submitted July 17, 1998; Revised May 24, 1999; Accepted June 9, 1999

Abstract. In this paper, we report the synthesis, the physical properties and the electrochemical features of the lithium nickel-cobalt oxide cathode materials prepared by a combustion method at moderate temperature. Structural properties were investigated by X-ray diffraction, Raman scattering and FTIR. Spectroscopic measurements show unambiguously that the final product is identified as a modified-spinel structure (Fd3m space group) with the stoichiometric formula $\text{Li}_2[\text{Ni}_{0.5}\text{Co}_{0.5}]_2\text{O}_4$. Electrochemical cells $\text{Li}/\text{Li}_2[\text{Ni}_{0.5}\text{Co}_{0.5}]_2\text{O}_4$ were fabricated using an organic electrolyte and their performances were tested. For a modified-spinel $\text{Li}_2[\text{Ni}_{0.5}\text{Co}_{0.5}]_2\text{O}_4$ structure the chemical diffusion coefficient of Li ions is around $10^{-10} \text{ cm}^2\text{s}$, which is lower than for a layered $\text{LiNi}_{0.5}\text{Co}_{0.5}\text{O}_2$ host matrix.

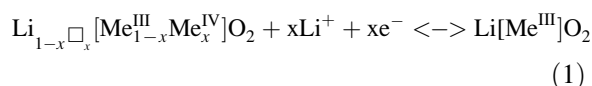
Keywords: Li-Ni-Co oxides, Raman, FTIR, electrochemical properties, lithium batteries

1. Introduction

Many lithium intercalated transition metal oxides have been studied as the positive electrode material used in high energy density rechargeable batteries. Research work in this area have focused the attention mainly on LiMn_2O_4 and LiMeO_2 (Me = Ni, Co) compounds synthesized by solid reaction using high temperature (HT) methods [1–9], which show higher operating voltages than the conventional 3-volt systems. These compounds crystallize in the spinel-type [10] and the $\alpha\text{-NaFeO}_2$ layered-type structure [11], respectively. Lithium cobaltate is one of the most advanced studied materials but some limitations are due to its high cost, moderate capacity and toxicity. Lithium nickelate is one of the most attractive materials for lithium-ion cells. However, non-stoichiometric $\text{Li}_x\text{Ni}_y^{(\text{II})}\text{Ni}_{1-y}^{(\text{III})}\text{O}_2$ oxides are usually obtained, nickel dioxide electrochemically formed from LiNiO_2 is quite active

for an organic electrolyte oxidation and the reaction is exothermic. Lithiated manganese oxide, LiMn_2O_4 , is exploited very much as a battery cathode in lithium-ion cells due to its availability, non toxicity, besides its low cost compared to its counterpart materials like LiCoO_2 and LiNiO_2 . However, the LiMn_2O_4 spinel phase exhibits lower capacity and the rechargeable capacity fades rapidly for deep charge-discharge cycles, particularly at high temperature (60°C).

A possible solution to reduce the above disadvantages is to utilize solid solutions of general formula $\text{LiNi}_{1-y}\text{Co}_y\text{O}_2$, which are isostructural with the layered oxide end-compounds and showed electrochemical features better than those of LiNiO_2 and LiCoO_2 [12–14]. The classical reaction in a Li/LiMeO_2 intercalation cell can be written as



which normally lies in between the voltage 4.5 and 3.0 V [6].

Synthesis routes for low temperature crystallized oxides, LT-Li(Ni,Co)O₂ have been reported [15–19]. This procedure allows a better mixing of the elements and thus a better reactivity of the mixture. Lower reaction temperature and shorter reaction time are then possible to yield a compound of high homogeneity and high specific area, but electrochemical tests showed that it did not exhibit superior specific capacity to the layered HT-Li(Ni,Co)O₂. It was reported that lithium extraction occurs at lower potential than for its HT-analogue [20].

In this paper, we report the synthesis and characterization of lithium nickel-cobalt (Li-Ni-Co) oxide cathode materials obtained by a synthetic combustion procedure at moderate temperature [21]. The structural properties have been characterized by X-ray diffraction and vibrational spectroscopies, i.e., Raman scattering and FTIR, which provide information on the local environment of atoms in the lattice. The final product with a modified-spinel structure (Fd3m space group) possesses the stoichiometric formula Li₂[Ni_{0.5}Co_{0.5}]₂O₄. The suitability of Li₂[Ni_{0.5}Co_{0.5}]₂O₄ as positive electrode was tested by fabricating a lithium cell in non-aqueous electrolyte and its electrochemical features as well as the lithium-ion diffusivity in the host matrix have been studied during the first charge of the Li//Li₂[Ni_{0.5}Co_{0.5}]₂O₄ cell.

2. Experimental

2.1. Preparation of the Li-Ni-Co Oxide

The Li-Ni-Co oxide samples were synthesized by combustion of aqueous solutions containing metal nitrates and urea in stoichiometric amounts [21,22]. The mixture of LiNO₃ with half the molecular weight of cobalt and nickel nitrates dissolved in an aqueous solution was evaporated to dryness. The stoichiometric composition of the metal nitrates and urea mixtures was calculated on the total oxidizing and reducing valencies of the oxidizer and fuel which released the energy at a maximum [21]. The mixtures, when rapidly calcined to 500°C for few hours, ignited and yielded the product of the composition LiNi_{0.5}Co_{0.5}O₂. The product obtained is black in

color with lustre. It is a fine grained material of micrometer size and the yield was above 95%.

2.2. Instruments

X-ray diffraction (XRD) patterns were obtained with a Philips PW1830 X-ray diffractometer using nickel-filtered Cu-K_{α1} radiation ($\lambda = 1.5406\text{\AA}$). The diffraction patterns were taken at room temperature in the range of $10^\circ < 2\theta < 80^\circ$ using step scans. The step size and the scan rate were set at 0.1 and 0.2 degree/min, respectively.

Room-temperature Raman scattering (RS) spectrum was collected in a quasi-backscattering configuration on the powder sample annealed at 500°C. A Jobin-Yvon model U 1000 double monochromator with holographic gratings and a computer-controlled photon-counting system was used. The laser light source was the 514.5 nm line radiation from a Spectra-Physics 2020 argon-ion laser. A RS spectrum is the average of 12 scans obtained with a spectral resolution of 2 cm^{-1} . Its RS spectrum was recorded with a low power laser excitation of 15 mW to prevent any decomposition of the sample. Fourier transform infrared (FTIR) spectrum was recorded using a Bruker IFS113v interferometer at a spectral resolution 2 cm^{-1} . In the far-infrared region, the spectrometer was equipped with a 3.5 μm -thick beam splitter, a global source, and a DTGS/PE detector. Samples were ground to fine powders painted onto polyethylene slabs.

2.3. Electrochemical Measurements

Electrochemical studies were carried out on the synthesized lithium nickel-cobalt oxide product annealed at 500°C in order to test its suitability as cathode-active material in high voltage lithium-containing batteries. The above tests were performed to measure quantitatively the energy content (capacity in mAh/g) the so-called electrochemical-capacity of the synthesized spinel product. The laboratory-scale Li//Li-Ni-Co oxide cells were fabricated employing a non-aqueous Li⁺ ion conducting organic electrolyte as follows. The typical composite cathode consisted of the mixture of lithium nickel-cobalt oxide powders, acetylene black and colloidal PTFE binder in the 90:5:5 weight ratio. The PTFE-acetylene black was used to provide good electrical conductivity as well as mechanical toughness between active grains. The

above mixture was pressed on to an expanded aluminium microgrid at a pressure of 500 MPa. This procedure yields circular pellet electrodes of 10 mm diameter. The pellets were then dried at 120°C in air. Celgard 2400 membrane was used as the separator between the cathode and the anode. The electrolyte was prepared by dissolving 1M LiPF_6 in 1:1 (v/v) mixture of ethylene carbonate (EC) and dimethyl carbonate (DMC), respectively. Electrodes and separators were soaked in the electrolyte before being housed in a Teflon laboratory-cell hardware. In order to assess their electrochemical performance, potentiostatic cyclic voltammograms were recorded at a slow scan mode in the potential range between 3.0 and 4.2 V using a Mac-Pile system.

3. Results and Discussion

3.1. Structural Considerations

Figure 1 shows the powder x-ray diffraction diagram of a lithium nickel-cobalt oxide sample prepared at 500°C. These XRD patterns appear to be similar to those reported in the literature [15]. They are dominated by a strong Bragg peak located at ca. $2\theta = 19^\circ$ and Bragg peaks with medium intensity at 36 and 44°. Considering the intensity and position of the Bragg peaks, it is well known that patterns can be indexed either to a rhombohedral unit cell (R3m) of a layered structure or, because the c/a ratio equals 4.90, to a face-centered cubic unit cell (Fd3m) of a spinel

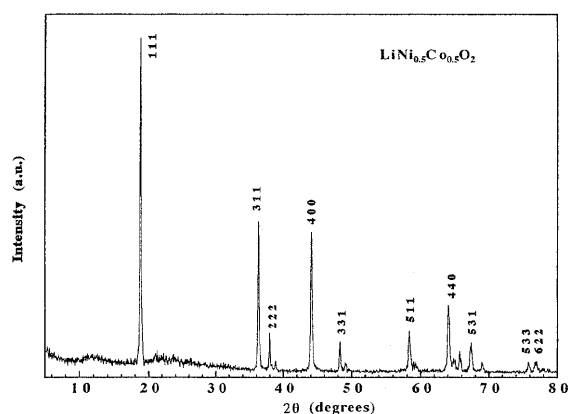


Fig. 1. Observed X-ray diffraction patterns of microcrystalline lithium nickel-cobalt oxide powders synthesized at 500°C. XRD peaks were indexed assuming the modified-spinel phase with Fd3m symmetry.

structure [15–18]. We decided to index the XRD diagram assuming a spinel-like structure with Fd3m space group because this assignment is in good accordance with our spectroscopic data, as shown herewith. Thus the stoichiometric formula of the final product should be $\text{Li}_2[\text{Ni}_{0.5}\text{Co}_{0.5}]_2\text{O}_4$, which is the fully lithiated phase of spinel.

It has been reported that if the synthesis of lithium cobaltate compounds is carried out at 400°C, then materials are produced with a modified structure and have different properties compared to their high-temperature analogues. They have spinel-like x-ray and neutron-diffraction patterns [23]. Our results suggest that $\text{Li}[\text{Ni}_{0.5}\text{Co}_{0.5}]\text{O}_2$ sample prepared at 500°C adopts also this structural modification; thus we observe the formation of the modified-spinel structure without any impurity phases and the XRD patterns match based on Fd3m space group analogous to $\text{Li}_2\text{Ti}_2\text{O}_4$ (i.e., $\text{Li}_2\text{NiCoO}_4$), in which all cations occupy octahedral sites. In this modified-spinel structure, the oxygen atoms occupy fully the 32e sites and Li and Co fully occupy the 16c and 16d octahedral interstices, respectively, with very little cation mixing. This is slightly different than the normal spinel structure of LiMn_2O_4 , in which Li fully occupies tetrahedral sites (Wyckoff position 8a in Fd3m).

The XRD peaks of $\text{Li}_2[\text{Ni}_{0.5}\text{Co}_{0.5}]_2\text{O}_4$ prepared at 500°C were indexed assuming the cubic lattice parameter with $a = 8.01\text{Å}$ (Table 1). The degree of crystallinity, i.e., domain size, was examined by measuring the full width at half maximum (FWHM) for (004) peak at ca. $2\theta = 44^\circ$, which is found to be very sensitive to the synthesis temperature. The domain size becomes quite small, about $1\ \mu\text{m}$, at 500°C, indicating the low lattice strain.

The Raman scattering (RS) and Fourier transform infrared (FTIR) spectra of the synthesized lithium nickel-cobalt oxide recorded at room temperature are shown in Figs. 2 and 3, respectively. The RS spectrum (Fig. 2) is dominated by a strong and broad band at ca. $621\ \text{cm}^{-1}$ with two shoulders at 574 and $647\ \text{cm}^{-1}$. Three bands with a medium intensity appear at ca. 492 , 439 and $371\ \text{cm}^{-1}$, while three bands having a weak intensity are observed at ca. 489 , 415 and $310\ \text{cm}^{-1}$. The FTIR absorption spectrum (Fig. 3) is dominated by two strong absorption bands at ca. 622 and $516\ \text{cm}^{-1}$. Three weak bands are observed in the low frequency region at ca. 450 , 261 and $220\ \text{cm}^{-1}$, and two shoulders are recorded at ca. 392 and $340\ \text{cm}^{-1}$. The RS and FTIR spectra of the layered

Table 1. Structural analysis of lithium nickel-cobalt oxide synthesized at 500°C. The Miller indexes are given assuming the $Fd\bar{3}m$ symmetry (cub.) and the $R\bar{3}m$ symmetry (hex.)

No.	d_{obs}	Intensity	$(hkl)_{\text{hex.}}$	$(hkl)_{\text{cub.}}$
1	4.711	100	003	111
2	2.471	44	101	113
3	2.367	12	006/102	222
4	2.053	42	104	004
5	1.883	9	105	133
6	1.578	12	107	115/333
7	1.450	19	108/110	044
8	1.390	9	113	135
9	1.254	3	021	336
10	1.239	3	202	226

$\text{LiNi}_{0.5}\text{Co}_{0.5}\text{O}_2$ phase ($R\bar{3}m$ space group) are also shown (Figs. 2 and 3). The preparation and characterization of this sample have been reported elsewhere [26]. It is a HT-Li(Ni,Co) O_2 phase made through melt impregnation technique, where anhydrous LiOH was mixed with stoichiometric amounts of NiO and Co_3O_4 and heat treated at 450°C for 8 h. The mixture was cooled to ambient temperature, and

ground to fine powder and heat treated at 750°C for 20 h. Both heat treatments were done under oxygen atmosphere. In this case, the layered $\text{LiNi}_{0.5}\text{Co}_{0.5}\text{O}_2$ material exhibits only two Raman-active modes at 480 and 586 cm^{-1} . A comparison of these spectra demonstrates clearly that the number of active modes is higher for the modified-spinel $\text{Li}_2[\text{Ni}_{0.5}\text{Co}_{0.5}]_2\text{O}_4$ structure than for the layered rhombohedral-like

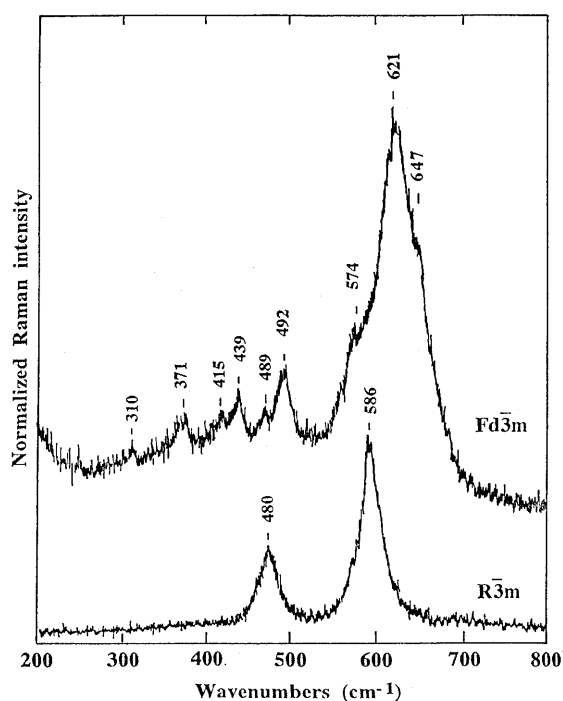


Fig. 2. Typical Raman scattering spectra recorded with the 514.5 nm line of an Ar-ion laser line at 15 mW power excitation. (a) $\text{Li}_2[\text{Ni}_{0.5}\text{Co}_{0.5}]_2\text{O}_4$ sample prepared by the combustion method at moderate temperature and (b) $\text{LiNi}_{0.5}\text{Co}_{0.5}\text{O}_2$ microcrystalline powder synthesized at high temperature.

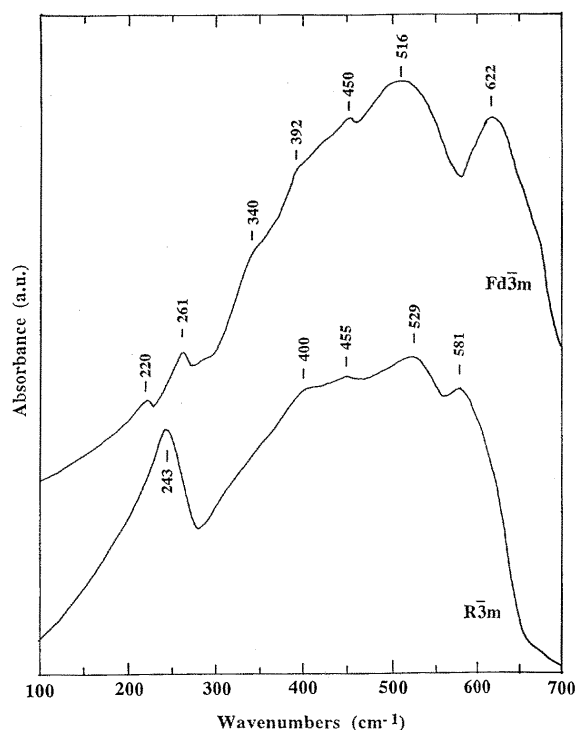


Fig. 3. Typical FTIR absorption spectra recorded on (a) $\text{Li}_2[\text{Ni}_{0.5}\text{Co}_{0.5}]_2\text{O}_4$ sample prepared by the combustion method at moderate temperature and (b) $\text{LiNi}_{0.5}\text{Co}_{0.5}\text{O}_2$ microcrystalline powder synthesized at high temperature.

$\text{LiNi}_{0.5}\text{Co}_{0.5}\text{O}_2$ phase. Because the crystallographic anomaly does not affect either the Raman or FTIR spectrum, we can definitely assume that the symmetry of the Li-Ni-Co oxide solid solution synthesized at 500°C is of $\text{Fd}\bar{3}\text{m}$.

The ideal $\alpha\text{-NaFeO}_2$ -type structure belongs to the $\text{R}\bar{3}\text{m}$ symmetry, for which the group factor analysis yields two Raman-active modes ($\text{A}_{1g} + \text{E}_g$) and four infrared-active modes ($2\text{A}_{2u} + 2\text{E}_u$). The ideal cubic spinel possesses $\text{Fd}\bar{3}\text{m}$ symmetry and has a general structural formula $\text{A}[\text{B}_2]\text{O}_4$, for which the group factor analysis yields nine optic modes [24]. Five modes are Raman active ($\text{A}_{1g} + \text{E}_g + 3\text{F}_{2g}$) and four are infrared active (F_{1u}). It is also convenient to analyze the vibrational spectra in terms of localized vibrations, considering the modified-spinel structure built of MeO_6 ($\text{Me} = \text{Ni}, \text{Co}$) and LiO_6 octahedra [25], for which the group factor analysis yields also nine optic modes. Spectroscopic features of a disordered compound will exhibit peak broadening due to the folding of the optical branches in the reduced Brillouin zone.

Vibrational spectra show unambiguously that the lithium nickel-cobalt oxide possesses a modified-spinel structure. The Raman band located at ca. 621 cm^{-1} can be viewed as the symmetric Me-O stretching vibration of MeO_6 groups. This band is assigned to the A_{1g} symmetry in the O_h^7 spectroscopic space group. Its broadening may be related with the cation-anion bond lengths and polyhedral distortion occurring in $\text{Li}_2[\text{Ni}_{0.5}\text{Co}_{0.5}]\text{O}_4$. The intensity of the shoulder located at 574 cm^{-1} increases upon lithium deintercalation. The RS peak at 492 cm^{-1} has the E_g symmetry, whereas the peaks located at lower frequency have the F_{2g} symmetry. The high-frequency bands of the FTIR absorption spectrum of $\text{Li}_2[\text{Ni}_{0.5}\text{Co}_{0.5}]\text{O}_4$ located at ca. 622 and 516 cm^{-1} are attributed to the asymmetric stretching modes of MeO_6 group, whereas the low-frequency bands at ca. 450 , 392 and 340 cm^{-1} are assigned to the bending modes of Me-O. Because FTIR spectroscopy is capable of probing directly the near neighbor environment of the cation, we can study the local environment of lithium ions in this material [27,28]. It has been also demonstrated that the IR resonant frequencies of alkali metal cations in their octahedral interstices in inorganic oxides are located in the frequency range $200\text{--}300\text{ cm}^{-1}$ [28,29]. Thus, the IR resonant frequency LiO_6 groups appears at 269 and 237 cm^{-1} in the LiCoO_2 and LiNiO_2 layered structures ($\text{R}\bar{3}\text{m}$ space group), respectively. This

leads to the frequency at ca. 261 cm^{-1} for the oscillation of the Li^+ ion with O^{2-} near neighbors in $\text{Li}_2[\text{Ni}_{0.5}\text{Co}_{0.5}]\text{O}_4$. The frequency of the vibrational modes and the analysis of the spectroscopic data of $\text{Li}_2[\text{Ni}_{0.5}\text{Co}_{0.5}]\text{O}_4$ are summarized in Table 2.

In the modified-spinel $\text{Li}_2[\text{Ni}_{0.5}\text{Co}_{0.5}]\text{O}_4$, the Ni^{III} and Co^{III} cations are considered as crystallographically equivalent (16d sites) in agreement with XRD data; then, occupation probabilities of 0.5 must be affected for each cation in 16d. Hence, a loss of translation invariance certainly occurs, due to local lattice distortions around the different Ni^{III} and Co^{III} cations. As a result, a breakdown in the Raman and IR selection rules is expected, which may explain the observation of broad bands (disorder) and the fact that more modes than expected are observed in the modified-spinel structure $\text{Li}_2[\text{Ni}_{0.5}\text{Co}_{0.5}]\text{O}_4$. On the other hand, a structural disorder of the layered oxide, which gives a more three dimensional character to the product, could induce a modified-spinel lattice. This structural disorder could have several origins such as lattice distortion around cations in the (Ni, Co) slabs, random distribution on the Ni, Co sites, heavy migration of transition metal within the predominantly lithium sites. It can be stated that Raman, which is sensitive only to the skin of the particle, could give signature close to spinel whereas bulk is still in layered form. As FTIR absorption measurements have shown the signature to modified-spinel bulk, this hypothesis is nearly improbable.

In conclusion, our investigations on the vibrational spectra of the lithium nickel-cobalt oxide compound have unambiguously determined the modified-spinel $\text{Li}_2[\text{Ni}_{0.5}\text{Co}_{0.5}]\text{O}_4$ structure of the material synthesized at 500°C . Analysis of the Raman scattering and FTIR absorption spectra has shown the modified-spinel oxide with $\text{Fd}\bar{3}\text{m}$ symmetry rather than the layered oxide with $\text{R}\bar{3}\text{m}$ symmetry. It was also demonstrated the local environment of cations against oxygen neighbors, i.e., lithium and transition-metal atoms reside in octahedral interstices of the modified-spinel matrix.

3.2. Electrochemical Charge-Discharge Features

The electrochemical behavior of synthesized spinel $\text{Li}_2[\text{Ni}_{0.5}\text{Co}_{0.5}]\text{O}_4$ was examined in lithium-containing test cells employing a non-aqueous electrolyte. The Li metal acted as both counter and reference electrodes, while $\text{Li}_2[\text{Ni}_{0.5}\text{Co}_{0.5}]\text{O}_4$ was

Table 2. Wavenumbers (in cm^{-1}), intensities^a, and assignments of the Raman-active and IR-active modes of the modified-spinel $\text{Li}_2[\text{Ni}_{0.5}\text{Co}_{0.5}]_2\text{O}_4$

Raman	Intensity	IR	Intensity	Assignment
250	w	220	w	$\nu(\text{Li-O})$
310	w	261	m	$\nu_2(\text{M-O})$
371	m	340	s	
415	w	392	w	$\nu(\text{Li-O}) + \nu(\text{M-O})$
439	m	450		$\nu(\text{Li-O}) + \nu(\text{M-O})$
489	w			
492	m	516	S	$\nu_4(\text{M-O})$
574	m			$\nu_3(\text{M-O})$
621	S	622	$\nu_1(\text{M-O})$	
647	s			

^aw = weak, m = medium, s = shoulder, S = strong.

treated as working electrode. The electrodes are separated by a porous membrane soaked in an electrolyte of 1M LiPF_6 in 1:1 (v/v) mixture of EC-DMC. To begin with electrochemical measurements, the samples were first characterized by cyclic voltammetry on $\text{Li}/\text{Li}_2[\text{Ni}_{0.5}\text{Co}_{0.5}]_2\text{O}_4$ cell. The voltammogram shown in Fig. 4 reveals a good reversibility of the cells containing spinel $\text{Li}_2[\text{Ni}_{0.5}\text{Co}_{0.5}]_2\text{O}_4$.

Figure 5 shows the first charge and discharge curves at 28°C for a $\text{Li}/\text{Li}_2[\text{Ni}_{0.5}\text{Co}_{0.5}]_2\text{O}_4$ non-aqueous cell operated under galvanostatic conditions. The open-circuit voltage of a freshly prepared cell was 2.9 V. The cell was charged and discharged at current density 0.05 mA/cm^2 , while the voltage is monitored between 3.0 and 4.0 V. During the charge at 0.05 mA/cm^2 the voltage profile is as follows: (i) the voltage rapidly increased to about 3.45 V, (ii) a plateau is observed at

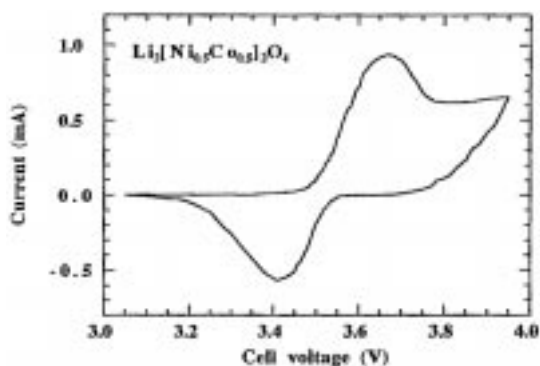


Fig. 4. Typical cyclic voltammogram vs. a pure lithium anode of $\text{Li}_2[\text{Ni}_{0.5}\text{Co}_{0.5}]_2\text{O}_4$ sample prepared by the combustion method at moderate temperature.

3.50 V, and (iii) then the voltage followed an ascending curve. In this voltage domain, the charge-discharge curves correspond to the voltage profiles characteristic of the $\text{LiNi}_{1-y}\text{Co}_y\text{O}_2$ cathode materials prepared at low temperature, in agreement with previous works [23]. From the variation of the cell potential for the complete cell (Fig. 5), one can distinguish the presence of two regions during the lithium insertion-extraction processes. The shape of the charge voltage curves indicates whether the delithiated $\text{Li}_{2(1-x)}[\text{Ni}_{0.5}\text{Co}_{0.5}]_2\text{O}_4$ exists as a two-phase compound in the range $0.6 \leq x \leq 1.0$. In this case the potential is expected to be essentially invariant with composition. The second region (for $x \leq 0.6$) is characterized by a compositional dependent voltage curve, where the charge/discharge voltage increases/decreases continu-

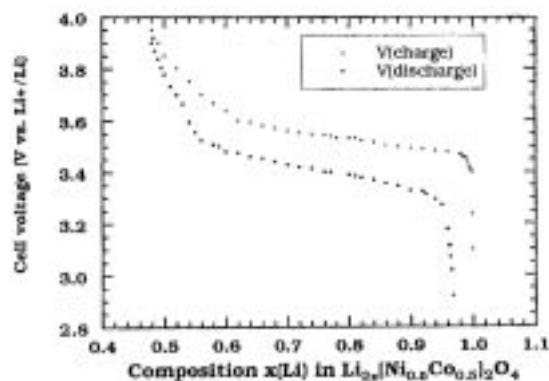


Fig. 5. Typical charge-discharge characteristics of $\text{Li}/\text{Li}_2[\text{Ni}_{0.5}\text{Co}_{0.5}]_2\text{O}_4$ non-aqueous cell employing the electrolyte of composition 1M LiPF_6 in EC-DMC.(1:1) at room temperature. Charge and discharge were obtained at current density 0.05 mA/cm^2 .

ously in the voltage range of 3.5–4.0 V. These results indicate that the loss of charge capacity occurs during the first cycle. The loss of charge capacity is about 8% in the first cycle, after which the cell cycles with more coulombic efficiency.

These results give only weak evidence that the electrochemical features of the modified-spinel compound are different than the pure layered phase. This behavior is attributed to the quasi-spinel phase in which the cations are located only in octahedral sites with the existence of cation mixing. However, the charge-discharge profiles of $\text{Li}_2[\text{Ni}_{0.5}\text{Co}_{0.5}]_2\text{O}_4$ positive electrodes prepared at moderate temperature are recorded at lower voltage than for high-temperature materials. This experimental fact is in good agreement with those reported in the literature [16–18]. The low capacity of the sample is also indicative of heavy migration of transition metal within the oxide slab (into the lithium sites), which gives a more three dimensional character to the product, consistent with both Raman and X-ray data.

Considering that the relaxation in the cell is primarily rate-limited by lithium diffusion in the oxide, we have studied its kinetics. Chemical diffusion coefficients (D^+) of lithium ions in $\text{Li}_2[\text{Ni}_{0.5}\text{Co}_{0.5}]_2\text{O}_4$ host material have been investigated as a function of the amount of lithium deintercalated in the domain of the galvanic cell reversibility. They were determined by the GITT method from the variation of the transient cell voltage vs. time during the relaxation period following a long discharge or charge [30]. D^+ was calculated assuming a uniform Li^+ distribution at any composition. As in an intercalated material, the charge rate capability of

$\text{Li}_2[\text{Ni}_{0.5}\text{Co}_{0.5}]_2\text{O}_4$ is greatly influenced by the chemical diffusion of Li ions in the host matrix of the oxide crystals. The chemical diffusion coefficients of Li^+ ions were reported to be in the range 10^{-8} – 10^{-9} cm^2/s for $0.1 \leq x \leq 1.0$ in Li_xCoO_2 [31]. Figure 6 shows the plot of the chemical diffusion coefficient as a function of lithium content in $\text{Li}_2[\text{Ni}_{0.5}\text{Co}_{0.5}]_2\text{O}_4$ during the first charge process (lithium deintercalation reaction). We observe that in the compositional range $0.48 \leq x \leq 1.0$, D^+ varies from 5×10^{-9} to 5×10^{-10} cm^2/s . So, these values are at least one order of magnitude lower than for LiCoO_2 . These features can be attributed to the disordered structural nature of the material indicating that the modified-spinel lattice exhibiting a lower rate capability than the rock-salt layered structure.

4. Conclusion

The positive electrode material $\text{LiNi}_{1-y}\text{Co}_y\text{O}_2$ ($y = 0.5$) has been synthesized using a combustion procedure at moderate temperature. Structural features suggested by X-ray diffraction show that lithium nickel-cobalt oxides have an essentially ideal cubic-closed-packed oxygen-ion lattice when prepared at 500°C . The quasi-spinel structure ($\text{Li}_2\text{NiCoO}_4$) is well-confirmed by vibrational spectroscopy, i.e., Raman scattering and FTIR absorption. The analysis of the Raman and FTIR absorption spectra shows that the local environment of the lithium nickel-cobalt oxide material is in good agreement with the classical structural model of $\text{Fd}3\text{m}$ space group. In the modified-spinel phase, lithium and transition-metal atoms occupy the octahedral 16d positions. The charge-discharge profiles of $\text{Li}_2[\text{Ni}_{0.5}\text{Co}_{0.5}]_2\text{O}_4$ positive electrodes prepared at moderate temperature were recorded at lower voltage than for high-temperature materials. For modified-spinel structure the chemical diffusion coefficient of Li ions is around 10^{-10} cm^2/s , which is lower than for a layered host matrix.

Acknowledgments

The authors would like to thank Dr. Saul Ziolkiewicz for valuable comments. This work was partially supported by the Indo-French Center for the Promotion of Advanced Research (IFCPAR) under grant No. 1408-2.

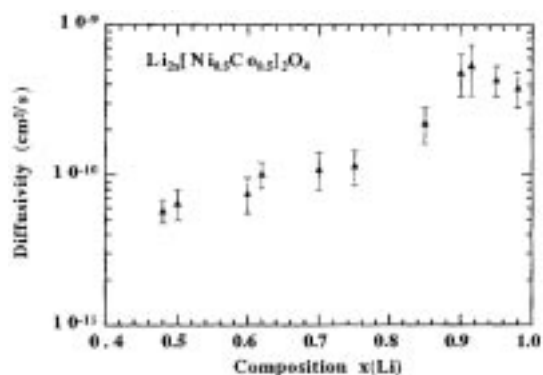


Fig. 6. Chemical diffusion coefficient of Li ions in $\text{Li}_2[\text{Ni}_{0.5}\text{Co}_{0.5}]_2\text{O}_4$ as a function of lithium concentration during the first charge.

References

1. J.C. Hunter, *J. Solid State Chem.*, **39**, 142 (1981).
2. M.M. Thackeray, W.I.F. David, P.G. Bruce, and J.B. Goodenough, *Mater. Res. Bull.*, **18**, 461 (1983).
3. J.M. Tarascon and D. Guyomard, *J. Electrochem. Soc.*, **138**, 2864 (1991).
4. T. Ohzuku, M. Kitagawa, and T. Hirai, *J. Electrochem. Soc.*, **137**, 769 (1990).
5. J.M. Tarascon, D. Guyomard, and G.L. Baker, *J. Power Sources*, **43–44**, 689 (1993).
6. K. Mizushima, P.C. Jones, P.J. Wiseman, and J.B. Goodenough, *Mater. Res. Bull.*, **15**, 783 (1980).
7. E. Rosen, J.N. Reimers, and J.R. Dahn, *Solid State Ionics*, **62**, 53 (1993).
8. P. Barboux, J.M. Tarascon, and F.K. Shokoohi, *J. Solid State Chem.*, **94**, 185 (1991).
9. I. Saadouné and C. Delmas, *J. Mater. Chem.*, **6**, 193 (1996).
10. Y. Gao and J.R. Dahn, *J. Electrochem. Soc.*, **143**, 100 (1996).
11. A. Ueda and T. Ohzuku, *J. Electrochem. Soc.*, **141**, 2013 (1994).
12. E. Zhecheva and R. Stoyanova, *Solid State Ionics*, **66**, 143 (1993).
13. T. Ohzuku, A. Ueda, M. Nagayama, Y. Iwakoshi, and H. Komori, *Electrochim. Acta.*, **38**, 1159 (1993).
14. A. Rougier, I. Saadouné, P. Gravereau, P. Willmann, and C. Delmas, *Solid State Ionics*, **90**, 63 (1996).
15. J. Gummow and M.M. Thackeray, *J. Electrochem. Soc.*, **140**, 3365 (1993).
16. J.N. Reimers, W. Li, E. Rossen, and J.R. Dahn, *Mat. Res. Soc. Symp. Proc.*, **293**, 3 (1993).
17. E. Rossen, J.N. Reimers, and J.R. Dahn, *Solid State Ionics*, **62**, 53 (1993).
18. B. Garcia, P. Barboux, F. Ribot, A. Kahn-Harari, L. Mazerolles, and N. Baffier, *Solid State Ionics*, **80**, 111 (1995).
19. W. Huang and R. Frech, *Solid State Ionics*, **86–88**, 395 (1996).
20. B. Garcia, J. Farcy, J.P. Pereira-Ramos, J. Perichon, and N. Baffier, *J. Power Sources*, **54**, 373 (1995).
21. S.S. Manoharan and K.C. Patil, *J. Am. Ceram. Soc.*, **75**, 1012 (1992).
22. S. Chitra, P. Kalyani, T. Mohan, R. Gangadharan, and C. Julien *A combustion procedure for the preparation of $\text{LiNi}_{1/2}\text{Co}_{1/2}\text{O}_2$ useful as the cathode material in the rechargeable lithium-ion rocking chair cells* Indian Patent (1999) under process.
23. J. Gummow and M.M. Thackeray, *Solid State Ionics*, **53–56**, 681 (1992).
24. G.C. Allen and M. Paul, *Appl. Spectrosc.*, **49**, 451 (1995).
25. C. Julien, A. Rougier, and G.A. Nazri, *Mat. Res. Soc. Symp. Proc.*, **453**, 647 (1997).
26. C. Julien, M. Massot, C. Perez-Vicente, E. Haro-Poniatowski, G.A. Nazri, and A. Rougier, *Mat. Res. Soc. Symp. Proc.*, **496**, 415 (1998).
27. C. Julien, C. Perez-Vicente, and G.A. Nazri, *Ionics*, **2**, 1 (1996).
28. J. Preudhomme and P. Tarte, *Spectrochim. Acta.*, **26A**, 747 (1970).
29. A. Rougier, G.A. Nazri, and C. Julien, *Ionics*, **3**, 170 (1997).
30. W. Weppner and R.A. Huggins, *J. Electrochem. Soc.*, **124**, 1569 (1977).
31. Y.M. Choi and S.I. Pyun, *Solid State Ionics*, **109**, 159 (1998).